Temperature dependence of the optical properties of CdTe

C. C. Kim, M. Daraselia, J. W. Garland, and S. Sivananthan
University of Illinois at Chicago, Microphysics Laboratory, Department of Physics, 845 W. Taylor, Chicago, Illinois 60607-7059
(Received 16 September 1996; revised manuscript received 3 February 1997)

CdTe(111)B films were grown on Si(100) substrates by molecular-beam epitaxy. Their spectral data were obtained from room temperature to 800 K by spectroscopic ellipsometry (SE) in the photon energy range from 1.3 eV to 6 eV. During the measurement, samples were heated inside a windowless chamber in which high-purity N_2 constantly flowed to minimize surface contamination. The spectral data revealed distinctive critical-point structures at E_0, $E_0+\Delta_0$, E_1, $E_1+\Delta_1$, $E_2(X)$, and $E_2(\Sigma)$. The spectral data were modeled. This enabled us to obtain the temperature dependence of the critical-point energies and linewidths. E_0, $E_0+\Delta_0$, E_1, $E_1+\Delta_1$, $E_2(X)$, and $E_2(\Sigma)$ decreased at the rate of 0.37, 0.34, 0.82, 0.64, 0.92, and 0.45 meV/K, respectively. All linewidths monotonically increased. The optical dielectric function was expressed as a function of temperature within and outside the experimental range. The results can be utilized for thermometry in order to determine the temperature of sample surfaces during growth. [S0163-1829(97)07832-6]

I. INTRODUCTION

CdTe has been an attractive candidate for use in various optoelectronic devices such as x-ray detectors, γ-ray detectors, and solar cells. It appears to be the most promising material for the next generation of soft-x-ray detectors.[1] Its major use thus far has been as a substrate for the epitaxial growth of $Hg_{1-x}Cd_xTe$, the most important semiconductor for infrared detection in the 8–12 μm range. Recently, CdTe has received more attention, since it has been grown on large-size Si substrates, despite a large lattice mismatch of the order of 20%.[2] This has made it possible to grow $Hg_{1-x}Cd_xTe$ as a subsequent layer and thus to fabricate monolithic integrated focal plane arrays.

A knowledge of the temperature dependence of the optical properties is necessary for many applications. For example, with such knowledge, *in situ* spectroscopic ellipsometry (SE) could be used to monitor or control the temperature during growth, just as it has been used to control the alloy composition and thickness.[3] SE is an excellent technique with which to determine the spectral dependence of the dielectric function, $\epsilon(\omega)=\epsilon_1(\omega)+i\epsilon_2(\omega)$. The experiment, however, yields only a set of points, $\{\epsilon(\omega_j)\}$; it does not give $\epsilon(\omega)$ as a function of critical-point (CP) energies E_i and linewidths Γ_i, or even of the photon energy $\hbar\omega$. But, SE data in conjunction with a suitable model for $\epsilon(\omega)$ allows one to determine the dielectric function as a function of photon energy, temperature and alloy composition. The optical properties of CdTe at room temperature have been reported by many authors,[4–8] but little data on their temperature dependence is available. No SE data on their temperature dependence have been reported previously.

CdTe films were grown on Si(100) by molecular-beam epitaxy.[2] Their spectral data were measured by SE in steps of 10 meV from 1.5 eV to 6 eV and in steps of 1 meV from 1.3 eV to 1.6 eV. The photon energy range of our SE setup, which was extended up to 6 eV,[9] was further extended below 1.5 eV. Although the accuracy obtained was not as good as that above 1.5 eV, it was sufficient to determine the band gap accurately. The temperature was varied in steps of about 50 K from room temperature to 800 K, above the typical growth temperature. During the measurement, samples were heated inside a windowless chamber in which high-purity N_2 constantly flowed to minimize surface contamination. The system performance was checked with respect to surface contamination during heating and during exposure to the atmosphere at room temperature. The effect of oxidization and surface roughness on the spectral data was removed to deduce the spectral data for bulk CdTe.

The optical dielectric function of bulk CdTe was modeled previously. The model satisfied the Kramers-Kronig relationship and enabled us to calculate the dielectric function beyond the spectral limits of our data and to predict roughly its temperature dependence.[10] The same model was used for this work, but with the temperature dependence. The model enabled the accurate determination of the CP parameters at E_0, $E_0+\Delta_0$, E_1, $E_1+\Delta_1$, $E_2(X)$, and $E_2(\Sigma)$ at each measurement temperature. This enabled the determination of these parameters, in particular, the CP energy $E_i(T)$ and linewidth $\Gamma_i(T)$ as functions of temperature. Our results show that E_0, $E_0+\Delta_0$, E_1, $E_1+\Delta_1$, $E_2(X)$, and $E_2(\Sigma)$ decrease at the rates 0.37, 0.34, 0.82, 0.64, 0.92, and 0.45 meV/K, respectively, as the temperature increases from 300 K to 700 K. This result is consistent with those previously reported by other authors at lower temperatures. The temperature dependence of the linewidths has not been reported previously. Our results show that all linewidths monotonically increase with temperature, as would be expected. The model also enabled us to calculate the dielectric function $\epsilon(\omega,T)$ as a function of temperature within and even outside the experimental range. Previously, we proposed a method to roughly predict the dielectric function at low and elevated temperatures from the room temperature spectral data.[10] Having determined spectral data at elevated temperatures, our predictions are compared with that data.

II. EXPERIMENT

CdTe films were grown by molecular-beam epitaxy (MBE). The details of the system were described in a previ-

ous paper.[11] The substrates used are 2-in diameter Si(001), which was tilted by 1°, 2°, and 4° toward [110] with respect to the surface. The growth conditions and sample quality were previously reported.[2] The spectral data were obtained with a spectroscopic ellipsometer. The heart of the system is a photoelastic modulator. It was improved previously to measure the dielectric function, especially in the photon energy range up to 6 eV, leading to the advantage that the E_2 structure which occurs around 5 eV was obtained. The experimental setup, acquisition procedure, method of data reduction and accuracy were reported previously.[12] The data were obtained using configuration II as defined by Bermudez and Ritz,[13] and zone averaging, which has been made easier with our system and which improves the accuracy.

More features were added to the existing system to control the sample temperature during measurement. A chamber was built to allow a constant flow of N_2 gas during the heating of the sample and thus to minimize surface oxidization. The chamber is made of aluminum and has only two holes, at the entrance and exit of the probing beam. The center positions of the holes are set to provide a 70° angle of incidence. The N_2 gas with high purity (99.995%) flowed from the bottom of the chamber up to those holes at constant pressure during the measurement. The sample holder is a copper block with a high-resistivity NiCr wire fed through a ceramic tube embedded in the block. The direct current power supply (HP6264B) for heating the block is connected to the temperature controller (Honeywell UDC2000), which maintains the desired temperature with a precision of ± 0.1 K. The thermocouple is K type and its contact point was located as close to the sample as possible for accurate determination of the temperature. The sample was firmly clamped to the copper block for the best heat transmission. Yao *et al.*[14] reported that the temperature difference from two thermocouples located near the sample was on the order of 10 K around 700 K. This suggests that at the highest temperature, 671 K, reported in this work the uncertainty would be less than 10 K. In the system, white light is first monochromatized and then used as a probing beam. The optical components and detectors are arranged inside a black box to prevent spurious rays from entering the detector. The heater at the sample position unfortunately becomes a source of light, which significantly affects the measurement. In order to discriminate the radiation of the heater from the true signal, the probing beam is chopped at a frequency of 500 Hz, and the detected beam is processed with a lock-in amplifier.

Temperature-dependent measurements have usually been performed with a vacuum chamber to avoid surface oxidization during heating,[14,15] whereas a windowless chamber was used for this study. The simplicity of a windowless chamber offers several advantages. The possible problems arising from a window in the beam path are eliminated. Besides, the signal-to-noise ratio is clearly better than that obtained with windows. This is crucial when numerical derivatives of the spectra are used for the accurate determination of critical-point parameters. With our system, however, the sample is covered with N_2 gas only during measurements and is exposed to the atmosphere between the measurements. This is due to the time constraint involved in the measurement. Each scan takes about an hour and four scans are needed to obtain the spectral data from 1.3 eV to 6 eV with the zone average

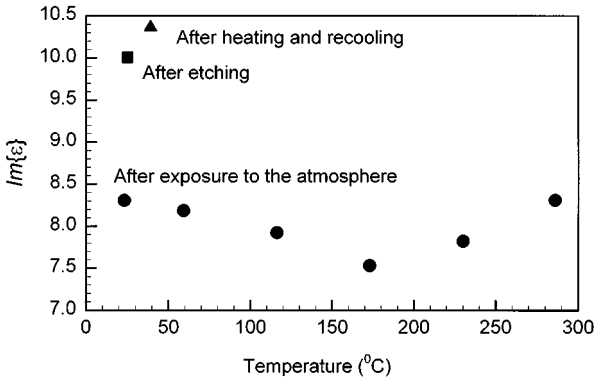

FIG. 1. Imaginary part of the dielectric constant for CdTe at 5 eV under various conditions. The square shows the value obtained at room temperature after chemical etching. The solid circles show the values obtained as temperature increases after the sample was first exposed to the atmosphere at room temperature. The triangle shows the value after cooling near room temperature.

at given temperature, permitting only two sets of data a day. Thus, the sample surface may not remain always in the same condition between the measurements. In addition, the system fails to maintain a good surface condition at very high temperature.

To take into account the overlayer effect present in our data, we first measured the optical constant at 5 eV under various conditions to examine the effect of native oxide, chemical etching, and annealing under N_2. Figure 1 shows the imaginary part of the dielectric constant at 5 eV, $\epsilon_2(5\text{eV})$. The photon energy 5 eV was chosen, because the dielectric constant at this energy is especially sensitive to the variation of the surface status.[16] A sample was chemically etched following the normal cleaning procedure for growth.[17] The treatment removed oxides from the surface as evidenced by the increase of the dielectric constant after etching. The square in Fig. 1 shows the value of $\epsilon_2(5\ \text{eV})$ after chemical etching. The sample was mounted inside the chamber and exposed to the atmosphere. The oxide layer did not grow significantly within one or two hours, but was eventually formed in a day. The decreased value of $\epsilon_2(5\ \text{eV})$ shown by the solid circle at room temperature was obtained after one day. A multilayer analysis of the SE data on this sample indicated that the oxide layer formed was only 2.4 nm thick, assuming the oxide dielectric function to be the same as that of SiO_2. That assumption certainly is good enough to conclude that the native oxide grows only to a thickness of order 2.5 nm (certainly less than 5 nm) if the sample is exposed to the atmosphere after etching. Then the sample was heated under an N_2 flow. As the temperature increased, the ϵ_2 values represented by the solid circles decreased due to the effect of temperature and possibly also further oxidization, but the trend changed above 173 °C. We suspect that desorption began to take place and its effect was larger than that of temperature as the temperature increased to 286 °C. At 286 °C the value of $\epsilon_2(5\ \text{eV})$ was monitored for two hours, and remained nearly constant, implying that the surface remained intact at this temperature. As the sample was cooled down, the value of $\epsilon_2(5\ \text{eV})$ increased steadily. At 39 °C, the value was even higher than the one obtained right after etching. Such an increased value sug-

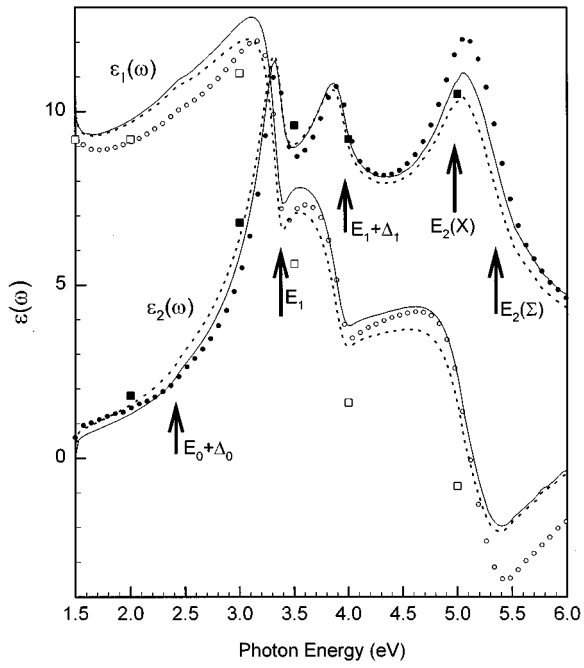

FIG. 2. Spectral data of CdTe at room temperature between 1.5 eV and 6 eV. The open and solid circles show the data by Arwin and Aspnes.[5] The open and solid squares show the data by Castaing *et al.*[8] The dotted lines are the data obtained after chemically etching the sample surface. The solid lines show the results after numerically removing 1 nm of SiO_2, which were chosen to represent the optical dielectric function of bulk CdTe at room temperature.

gests the removal of an overlayer.[16] Approximating the dielectric function of the overlayer by that of SiO_2, the observed change corresponds to the removal of a thickness of 0.5 nm. Another possibility is a change in surface morphology due to the heat treatment. If the overlayer was a surface roughness with a void fraction 0.5, such a change corresponds to the removal of 0.5 nm of roughness. In any case, the result shown by the triangle in Fig. 1 suggests that a more ideal surface might be prepared through heat treatment, but this question is beyond the scope of this paper. The results show that a windowless chamber in conjunction with the constant flow of N_2 not only is capable of keeping the surface intact, but also removes partially any oxide layer during the heating, so long as the sample temperature is not raised too high. The surface, however, begins to react strongly with the surroundings as the temperature increases beyond 400 °C. The surface was totally damaged at temperatures above 500 °C.

Our data at room temperature were obtained right after chemical etching[17] with N_2 covering the surface, known to be the best procedure to obtain room-temperature data.[16] The dotted lines in Fig. 2 show the data in steps of 10 meV from 1.5 eV to 6 eV. As pointed out above, etching alone might not have completely removed the overlayer from our sample. We have numerically removed the effect of an overlayer equivalent to 1 nm of SiO_2 from the data represented by the dotted lines. Of course, any oxide present on CdTe has a dielectric function different from that of SiO_2. The choice was made for the following reasons. The dielectric functions for the oxides of Cd and Te are not known. The choice of oxide dielectric function is not critical if the oxide thickness is left as a free parameter in one's analysis; as we have found in other investigations and as has been pointed out by Wakagi *et al.*,[18] the oxide thickness found in the analysis changes in such a way as to largely cancel out changes in the oxide dielectric function. In addition, our test for numerically removing the oxide layer of CdTe showed that the dielectric function of SiO_2 leads to the smaller rms value than that of the typical compound oxide $GaAsO_2$ once the oxide thickness is left as a free parameter. The resultant $\epsilon(\omega)$ values were chosen to represent the optical dielectric function of bulk CdTe at room temperature, as shown by the solid lines in Fig. 2. Although 1 nm is a reasonable thickness to assume, the actual overlayer thickness is not well defined by the SE data. We can say with any confidence only that it lies between zero and about 2 nm. However, the most important parameters determined from the analysis of our SE data, the critical-point energies and linewidths as functions of temperature, depend only weakly on our choice of overlayer thickness and on the nature of the sample surface, as is shown in Sec. IV. The data are compared with that of Arwin and Aspnes[5] and with the recently published data of Castaing *et al.*[8] The open and solid circles show the data reported by Arwin and Aspnes. The open and closed squares show the data of Castaing *et al.*, where the data are obtained from the graphs at selected temperatures. Our data show the same critical point structures as do those of Arwin and Aspnes, and our data for $\epsilon(\omega_2)$ are less noisy than theirs below 2.0 eV. The rms average difference between our data and theirs is 10%, with the largest differences occurring around the E_2 region and below the E_1 region. Our values for $\epsilon_2(\omega)$ are lower than those of Arwin and Aspnes in both regions. Otherwise, it would be deduced that the difference is mainly caused by an overlayer present in our sample. The opposite changes in magnitude in two different regions suggests that other factors, such as material quality, also contributed to the difference. The rms difference between the data of Castaing *et al.* and either our data or that of Arwin and Aspnes is substantially larger than that between our data and that of Arwin and Aspnes. Thus, the data of Castaing *et al.* is of little use in evaluating our data.

Figure 3 shows the spectral data of CdTe at selected temperatures—room temperature, 389 K, 503 K, 615 K, and 727 K. The solid and dash-dotted lines show the spectral data at room temperature and at 727 K, respectively. The dotted lines show the data taken in between. All the data were obtained in steps of 10 meV from 1.5 eV to 6 eV. The original data showed the effect of an overlayer. From the data shown in Fig. 1 and discussed above, the overlayer was assumed to be desorbed with increasing temperature, with the desorption becoming complete at 671 K. Thus, no overlayer correction was made at or above that temperature. It was also assumed that the maximum value of $\epsilon_1(\omega)$ in the E_1 region should linearly decrease with increasing temperature up to 671 K, following the trend shown by the temperature-dependent spectral data of GaAs.[19] This assumption allowed us to find the overlayer thickness $d_o(T)$ from room temperature up to 671 K, by numerically removing the effect of an assumed overlayer of SiO_2 from our data at each temperature and adjusting the assumed overlayer thickness to obtain the desired maximum value of $\epsilon_1(\omega)$. The values for d_o calculated

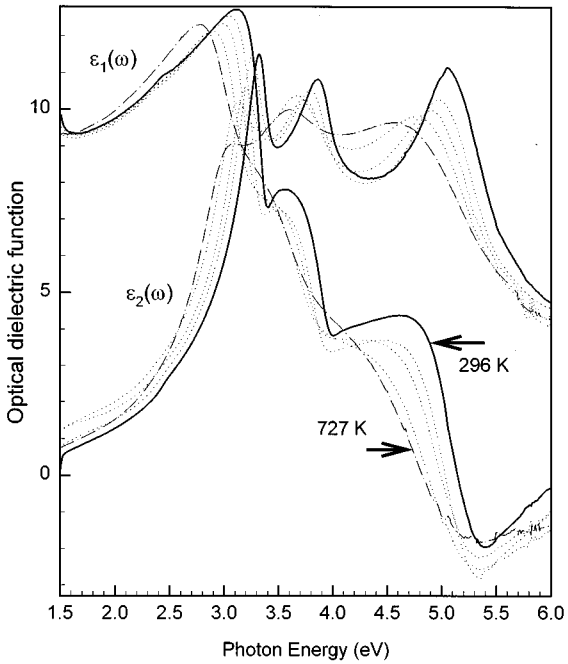

FIG. 3. Spectral data of CdTe at 296 K, 389 K, 503 K, 615 K, and 727 K. The data was measured in steps of 10 meV from 1.5 eV to 6 eV. The solid lines show the room-temperature data. The dashed lines show the data at 727 K. The intermediate-temperature data are shown by the dotted lines.

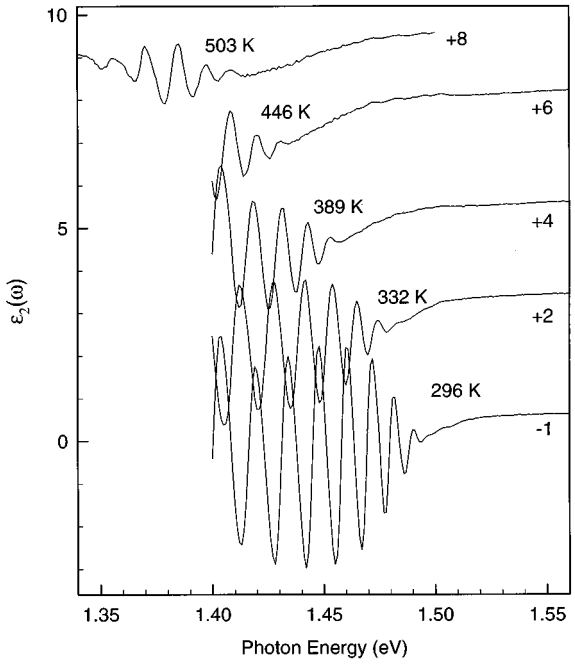

FIG. 4. Spectral data of CdTe at selected temperatures. The data were measured in steps of 1 meV between 1.3 eV and 1.6 eV. Most data were taken from 1.4 eV to 1.6 eV, except for those at 503 K, which were taken from 1.3 eV to 1.5 eV to cover the band gap below 1.4 eV. For ease of viewing the values of $\epsilon_2(\omega)$ are displaced vertically by the integer amounts shown near the right-hand end of each curve.

in this way are listed in Table I. The results indicate that the oxidation process is more prevailing than the desorption process up to 446 K, and the desorption process takes over the oxidation process beyond that temperature to 671 K. An alteration of the surface was shown in the spectral data taken above 727 K. The values for ϵ_2 between 1.5 eV and 2 eV should increase monotonically as temperature increases if the surface is unchanged, because the critical-point energies all decrease monotonically with increasing temperature. This was not the case for the spectral data taken above 671 K, where the values in that energy region decreased instead of increasing. Such a behavior could arise from a Fabry-Perot interference near the band gap, if a thin film began to form on the surface. It also could be caused by the loss of constituent atoms or by a strong reaction of the surface with surrounding atoms at high temperature. At 840 K the spectral data did not show any signature of the CP structures for CdTe, which implied that the surface was totally altered.

TABLE I. Values used for the overlayer thickness d_o at selected temperatures.

T (K)	d_o (nm)
296	1.0
332	2.9
389	3.2
446	4.5
503	3.2
558	1.6
615	0.6
671	0.0

Even after cooling to room temperature, the spectral data of CdTe were not restored. For these reasons, data taken beyond 671 K were not considered.

Spectral data are normally measured from 1.5 eV to 6 eV in our system. The lower limit is set by the rapid decrease of the quantum efficiency of the photomultiplier tube (PMT) below 1.5 eV. Since the band gap of CdTe at room temperature is around 1.5 eV and decreases as temperature increases, a special effort was made to make a measurement down to 1.3 eV. In our system, the current from the PMT is kept constant during the measurement through the feedback loop.[9] This constant value was lowered by a factor 10 for the region below 1.5 eV to compensate for the weaker response of the PMT than that in the normal scanning region. Although the data in the lower region failed to provide as accurate information on the optical properties as those in the normal scanning region, they did give reliable values for the band gap. Figure 4 shows the imaginary part of the dielectric function at various temperatures. The Fabry-Perot interference shown below the band gap is a typical signature of a film-substrate system. The band gap decreases monotonically as temperature increases. The amplitude of the Fabry-Perot interference also monotonically decreases, indicating that the absorption coefficient below the band gap increases as temperature increases. The real part of the dielectric function showed a similar trend. The data up to 446 K were taken in steps of 1 meV from 1.4 eV to 1.6 eV. The data at 503 K were taken from 1.3 eV to 1.5 eV so as to cover the range of the band gap. From the data at 503 K, in which the Fabry-Perot interference appears, but diminishes below 1.37 eV, we concluded that the data below 1.37 eV could not be trusted. This

prevented the measurement of the temperature dependence of the band gap above 503 K.

III. THEORY

The optical dielectric function of solid state materials with Lorentzian line broadening is given by the equation[12,20]

$$\epsilon(\omega)=1-\frac{8\pi\hbar^2e^2}{m^2}\int\frac{W(E)dE}{E^2}\times\left[\frac{1}{\hbar\omega-E+i\Gamma}-\frac{1}{\hbar\omega+E+i\Gamma}\right], \tag{1}$$

where

$$W(E)=\sum_{c,v}W_{cv}(E)=\sum_{c,v}P_{cv}(E)^2J_{cv}(E),$$

c and v stand for conduction and valence bands, respectively, $E\equiv E_{cv}(\mathbf{k})$ is the energy difference between a pair of bands at the point $\mathbf{k}$ in the Brillouin zone, $J_{cv}(E)$ is the joint density of states between the pair of bands, and $P_{cv}(E)$ is the weighted-average matrix element of the momentum operator between states differing in energy by E. Similarly, the optical dielectric function of solid-state materials with Gaussian broadening is given by the equation

$$\epsilon(\omega)=1+i\frac{8\pi\hbar^2e^2}{m^2}\int\frac{W(E)dE}{E^2}\left[\int_0^\infty ds e^{i(\hbar\omega-E+2i\tau^2s)s}-\int_0^\infty ds e^{i(\hbar\omega+E+2i\tau^2s)s}\right], \tag{2}$$

where τ is the root-mean-square scattering t matrix. Our model is based on Eqs. (1) and (2).

An analytical expression for the dielectric function was previously constructed to model the spectral data of CdTe at room temperature.[10] Briefly, a simple functional representation was constructed for $W(E)$. It consisted of five segments with the divisions naturally occurring at critical points with two-dimensional discontinuities. It fully satisfied the CP behavior with no artificial cutoffs. For the case of Lorentzian line broadening, the substitution of $W(E)$ into Eq. (1) led to the equation

$$\epsilon(\omega)=1-\sum_n\left[(p_nH_n+q_nF_n+r_nH_n\prime)_{\mathrm{I}}+(p_nG_n+q_nK_n)_{\mathrm{II}}+(p_nG_n+q_nK_n)_{\mathrm{III}}+(p_nG_n)_{\mathrm{IV}}+(p_nG_n+q_nH_n+r_nH_n\prime)_{\mathrm{V}}\right], \tag{3}$$

where the primes on H_n refer to the $E_0+\Delta_0$ CP in energy segment I and to an M_0-type CP added in segment V at 7.5 eV to better mimic $W(E)$ above 6 eV, the upper limit of our data. Here, H_n, F_n, G_n, and K_n are functions of ω as defined in a previous paper,[12] and p_n, q_n, and r_n are constants. The case of Gaussian line broadening was considered in a later paper,[10] and was shown to improve the calculation of $\epsilon_2(\omega)$ below the band gap. For brevity, this numerically much more complicated case is not considered in this work. Equation (3) was extended to model the temperature-dependent spectral data, since no significant qualitative change in the band structure is expected as temperature increases. Thus, a model

$$\epsilon(\omega,T)=1-\sum_n\left[\{p_n(T)H_n(T)+q_n(T)F_n(T)+r_n(T)H_n'(T)\}_{\mathrm{I}}+\{p_n(T)G_n(T)+q_n(T)K_n(T)\}_{\mathrm{II}}+\{p_n(T)G_n(T)+q_n(T)K_n(T)\}_{\mathrm{III}}+\{p_n(T)G_n(T)\}_{\mathrm{IV}}+\{p_n(T)G_n(T)+q_nH_n(T)+r_nH_n'(T)\}_{\mathrm{V}}\right] \tag{4}$$

was established by replacing the constant terms in Eq. (3) by polynomial functions of temperature and by permitting the variation of CP energies and linewidths in H_n, F_n, G_n, and K_n as functions of temperature.

The parameters in the model were determined by fitting the model to the spectral data and/or its derivatives. The fit was performed by minimizing the root-mean-square (rms) fractional error

$$\sigma=\frac{1}{4}\sum_{n=0}^{n=3}\sigma_n, \tag{5}$$

where

$$\sigma_n^2=\frac{\sum_j|[f_j]_{\mathrm{num}}^{(n)}-[s_j]_{\mathrm{num}}^{(n)}|^2}{\sum_j|[s_j]_{\mathrm{num}}^{(n)}|^2}, \tag{6}$$

f_j denotes a value obtained from our theoretical model, s_j denotes the data, the superscript n denotes an nth-order derivative, and the subscript num denotes numerical differentiation. The numerical differentiation is performed using a formula suggested by Savitz and Golay.[21] Notice that the numerical differentiation is applied both to the model and to the data so as to compensate for numerical distortion.[22,23]

Having determined a model and fitting procedure, the spectral data $L(\omega_j,T)$ were modeled in two steps. The first step was to determine the values for E_i and Γ_i from the spectral data at each temperature. The derivative spectra were used, except for the CP at E_0, since they had enhanced CP structures and made the accurate determination of CP parameters possible. The number of free coefficients among the $p_{\nu,n}$, $q_{\nu,n}$, and $r_{\nu,n}$ where $\nu=\mathrm{I},\ldots,\mathrm{V}$ denotes an energy segment was reduced to the minimum number required to fit only the second and third derivatives of the spectral data. Furthermore, each critical-point region was fit separately if its CP structure was well separated from the others in the derivative spectra. The results were used in determining $E_i(T)$ and $\Gamma_i(T)$. In the second step the $p_{n,\nu}(T)$ and $q_{n,\nu}(T)$ were redetermined by minimizing σ_0^2, using the values for $E_i(T)$ and $\Gamma_i(T)$ determined in the first step. This was done in order to obtain a best fit of $\epsilon(\omega_j,T)$ to $L(\omega_j,T)$ with the $E_i(T)$ and $\Gamma_i(T)$ fixed at their correct values. The second step was very quick because $\epsilon(\omega,T)$ is a linear function of the constant terms, so that they are determined exactly in only one iteration.

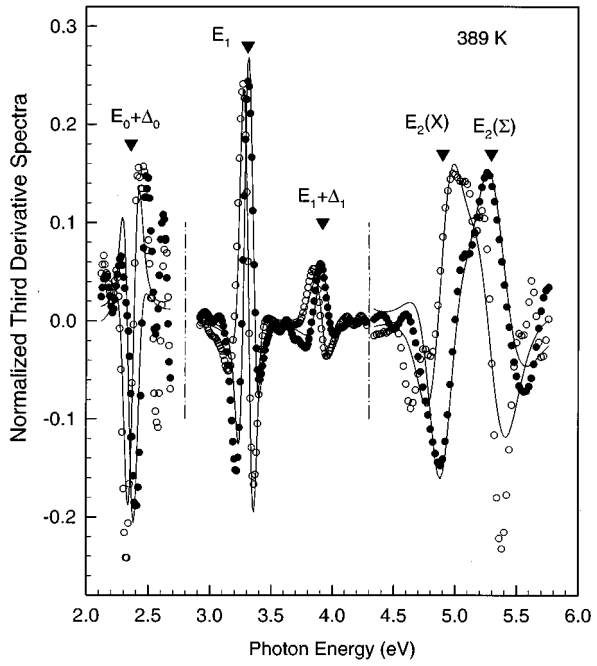

FIG. 5. Fit to the normalized third derivative spectra. The open (○) and closed (●) circles show their real and imaginary parts, respectively. The solid lines show the resultant fits. The dash-dotted lines show the boundaries between the energy segments fit independently. The inverted triangles denote the CP energy.

IV. CRITICAL-POINT ENERGIES AND LINEWIDTHS

Figure 5 shows one of the results performed in the first step in evaluating the E_i and Γ_i. For brevity only the normalized third derivative spectra at 389 K,

$$\frac{[L(\omega_j,389)]^{(3)}_{\rm num}}{\sqrt{\Sigma_j([L(\omega_j,389)]^{(3)}_{\rm num})^2}}, \tag{7}$$

and its fit are shown in this figure. The range between 1.5 eV and 6 eV was divided into three regions during the fit, since the CP structures were well isolated from one another and such a division made convergence faster. The interval between data points during the numerical differentiation was 10 meV in the region around $E_0+\Delta_0$, E_1 and $E_1+\Delta_1$, whereas the interval used around the E_2 region was 20 meV to improve the signal-to-noise ratio in the numerically differentiated signal. The dash-dotted lines show the boundaries between the divisions. For each CP, only one or two free parameters were used in addition to E_i and Γ_i. For this fit, $(\sigma_2+\sigma_3)/2$ from the $E_0+\Delta_0$, E_1 and E_2 region was 63%, 31%, and 35%, respectively. The large value from the $E_0+\Delta_0$ region was due to the weak structure and hence the small signal-to-noise ratio. The fractional error in the fits, as well as the uncertainties in the values obtained, generally increased as temperature increased, because the signal-to-noise ratio decreased, partially because the critical-point structure was diminished and altered by the effect of temperature. However, the fittings yield precise values for some of the CP energies, with uncertainties only of order $\pm 1-2$ meV for E_0 and E_1 at room temperature, under the assumption of uncertainties of order 1% in each measured datum, and only about ± 4 meV at 671 K. The least well-determined CP energy is $E_2(\Sigma)$, which can have an uncertainty as large as ± 12 meV at room temperature and ± 25 meV at 671 K.

The values obtained for the CP energies and linewidths are much less sensitive to sample overlayers and surface imperfection, to bulk sample quality, and to instrumentation than are the values of $\epsilon_1(\omega)$ and $\epsilon_2(\omega)$. However, they do depend weakly on these factors. In order to test the magnitude of the dependence of the E_i and Γ_i on such factors, we applied the procedure outlined above to find the E_i and Γ_i for three different sets of room-temperature CdTe spectral data. We chose the spectral data, $L^A(\omega_j)$, of Arwin and Aspnes[5] for bulk CdTe, our spectral data, $L(\omega_j,296)$, and spectral data, $L^{ox}(\omega_j,296)$, obtained on our sample after it was oxidized by exposure to the atmosphere, with a native oxide that approximately corresponded to 3.5 nm of SiO_2. The results obtained are shown in Table II. The oxide layer shifted the values found for $E_0+\Delta_0$ and E_1 by only 2 meV and 4 meV, respectively, and the values of the higher-energy critical points by no more than 10 meV. The differences between the values of $E_0+\Delta_0$ and E_1 found from $L^A(\omega_j)$ and from our data, $L(\omega_j,296)$, are similar to those induced by oxidation for $E_0+\Delta_0$ and E_1 but are larger at higher

TABLE II. Comparison of the critical-point energies and linewidths obtained from different spectral data at room temperature. They are determined by the method described in Sec. IV. The values are given in units of eV. The values of Γ for E_0 and $E_0+\Delta_0$ could not be found from $L^A(\omega_j)$ and were fixed at 50 meV during the fit.

CP parameters	$L^A(\omega_j)$	$L(\omega_j,296)$	$L^{ox}(\omega_j,296)$
$E_0+\Delta_0$	2.410	2.412	2.410
E_1	3.366	3.363	3.359
$E_1+\Delta_1$	3.985	3.959	3.950
$E_2(X)$	4.984	4.964	4.974
$E_2(\Sigma)$	5.400	5.348	5.355
$\Gamma_{E_0+\Delta_0}$		0.027	0.023
Γ_{E_1}		0.044	0.049
$\Gamma_{E_1+\Delta_1}$	0.098	0.081	0.091
$\Gamma_{E_2(X)}$	0.165	0.157	0.132
$\Gamma_{E_2(\Sigma)}$	0.233	0.257	0.225

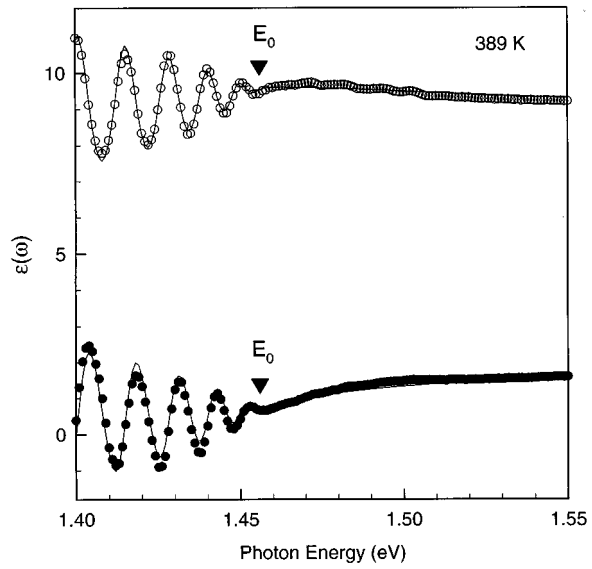

FIG. 6. Fit to $L(\omega_j,389)$ between 1.4 eV and 1.6 eV. The open (○) and closed (●) circles show the real and imaginary parts of $L(\omega_j,389)$, respectively. The solid lines show the resultant fits. The inverted triangles denote the value of the energy gap.

energies. The differences between the linewidths found from the three different spectra were two to three times as large as the differences between the CP energies and were of the order of 15% of the observed linewidths.

We conclude from the results shown in Table II that our uncertainty in the state of the CdTe surface during our measurements, which is substantially smaller than a 3.5-nm uncertainty in oxide thickness, leads to an uncertainty not much greater than ± 1 meV in $E_0+\Delta_0$ and E_1, and less than ± 4 meV in the higher CP energies. These uncertainties are very small in comparison with the temperature dependence of the CP energies. The corresponding uncertainties in the values of the CP linewidths, although larger, also are small in comparison with the temperature dependence of the linewidths.

The CP values at E_0 were determined in a different fashion from those for other critical points. The spectral data were used for the fit instead of their derivatives, because the Fabry-Perot interference below the band gap allowed the accurate determination of the CP parameters. In constructing the model, an overlayer-film-substrate system was assumed instead of a bulk system. The appropriate formula for the three-phase system has been well established.[24] The dielectric function for the Si substrate was obtained from the work by Edwards[25] and the dielectric function of the overlayer was approximated by that of SiO_2. The thicknesses were treated as parameters. The model for CdTe was

$$\epsilon(\omega)=1-p_0H_0+a+b\hbar\omega, \tag{8}$$

which was obtained from Eq. (1), considering only the CP structure at E_0. Notice, however, that the real quantity $a+b\hbar\omega$, with a and b variable parameters, was added to compensate for the oversimplification of the joint density of states above the band gap. This was sufficient to compensate for the contribution coming from the joint density of states above the band gap. For illustration, Fig. 6 shows the spectral data at 389 K, $L(\omega_j,389)$, and its fit. The open and solid

TABLE III. Values of the CP energies at selected temperatures. The CP energies were determined by the method described in Sec. IV. The values are given in units of eV for the CP energies.

T (K)	E_0	$E_0+\Delta_0$	E_1	$E_1+\Delta_1$	$E_2(X)$	$E_2(\Sigma)$
296	1.493	2.412	3.363	3.959	4.964	5.348
332	1.476	2.397	3.338	3.939	4.957	5.352
389	1.456	2.360	3.297	3.904	4.900	5.295
446	1.436	2.339	3.253	3.870	4.855	5.237
503	1.416	2.320	3.209	3.827	4.794	5.235
558		2.308	3.163	3.790	4.723	5.226
615		2.301	3.101	3.743	4.691	5.205
671		2.281	3.055	3.735	4.636	5.189

circles show the spectral data and the solid lines show the fit with $\sigma_0=7.5\%$, which led to $E_0=1.456$ eV, $\Gamma_0=5.7$ meV and a film thickness of 10.054 μm.

Table III shows the values found for the E_i at selected temperatures. The solid circles in Fig. 7 show those values. The value for E_0 at room temperature varies from 1.47 eV to 1.55 eV in the literature.[26] Our value, $E_0=1.493$ eV, is within this range. The values for the E_i monotonically decrease as the temperature increases. Table IV shows the values found for the Γ_i at selected temperatures. The results show that, as expected, the critical-point linewidths increase monotonically as temperature increases, within the uncertainty of their determination. The value for $\Gamma_{E_2(\Sigma)}$ is not shown in the table. Several factors made it difficult to treat $\Gamma_{E_2(\Sigma)}$ as a free parameter above room temperature. For one,

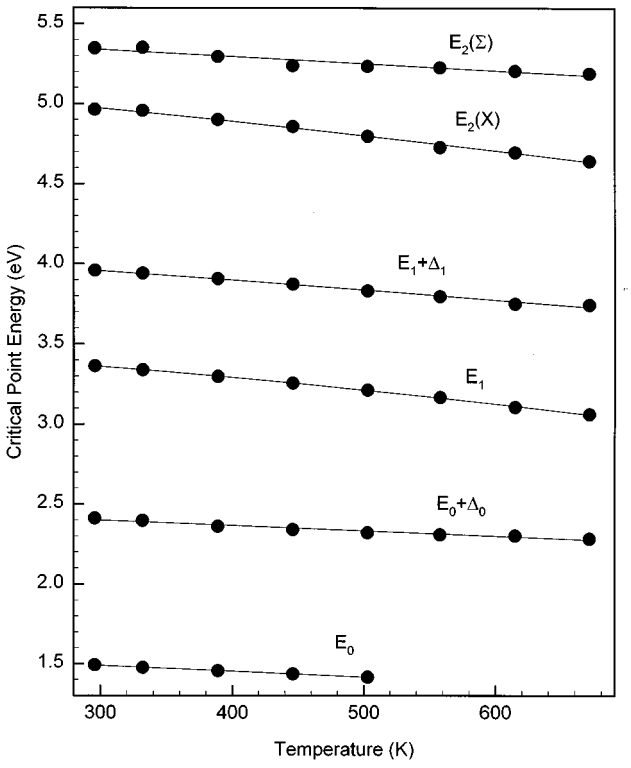

FIG. 7. CP energies as a function of temperature. The symbols show the values determined from fitting the data. The solid lines represent the fit by Eq. (10).

TABLE IV. Values of the critical-point linewidths at selected temperatures. They are determined by the method described in Sec. IV. The values are given in units of meV.

T (K)	Γ_{E_0}	$\Gamma_{E_0+\Delta_0}$	Γ_{E_1}	$\Gamma_{E_1+\Delta_1}$	$\Gamma_{E_2(X)}$
296	5.5	27	44	81	157
332	3.1	38	49	89	159
389	3.7	35	56	101	189
446	7.0	35	59	106	203
503	11.1	36	65	115	237
558		34	73	127	258
615		40	82	142	294
671		57	88	156	295

the signal-to-noise ratio decreased with increasing temperature. Also, the linewidth values and critical-point energy value in our fittings strongly interacted with one another because the separation between $E_2(X)$ and $E_2(\Sigma)$ became as small as the sum $\Gamma_{E_2(X)}+\Gamma_{E_2(\Sigma)}$ at higher temperatures. At room temperature the ratio of $\Gamma_{E_2(\Sigma)}$ to $\Gamma_{E_2(X)}$ was found to be 1.64. Because the ratio of linewidths was found to be approximately independent of temperature for any two critical points (other than E_0) at which $\Gamma_i(T)$ was determined, it was assumed that the ratio $\Gamma_{E_2(\Sigma)}/\Gamma_{E_2(X)}$ is equal to 1.64, independent of temperature over the temperature range studied.

The temperature dependence of the E_i can be described by Varshni's empirical relation[27]

$$E_i(T)=E_i(0)-\frac{\alpha_i T^2}{T+\beta_i}, \tag{9}$$

which describes well the temperature dependence of the E_i for GaAs.[28] However, the values of β_i for CdTe are expected to be very small, given the small Debye temperature $\Theta_D=158$ K for CdTe.[29] According to the model of Manoogian and Woolley,[30] $\beta=0.375\Theta_D$, which gives $\beta=59$ K for CdTe. Taking $\beta\propto\Theta_D$ and using the values $\beta_{E_0}=225$ K (Ref. 28) and $\Theta_D=344$ K (Ref. 31) for GaAs, one finds $\beta=0.654\Theta_D$, which gives $\beta=103$ K for CdTe. Therefore, because our results are limited to the range 296 K $\leqslant T\leqslant$ 671 K in which T is much greater than the expected value of β, we first fit our values for $E_i(T)$ using the linear equation

$$E_i(T)=E_i^{(0)}-\eta_i T, \tag{10}$$

valid for $T\gg\beta_i$. The fits to Eq. (10) are shown in Fig. 7; the resultant values of $E_i^{(0)}$ and $dE_i/dT=-\eta_i$ and the standard deviation, δ_i, are shown in Table V. Here, $E_i^{(0)}$ should be greater than $E_i(0)$, the zero-temperature value of E_i, because Eq. (10) must be replaced by Eq. (9) at low temperatures.

Table V displays two surprises. The more obvious one is that the values of η_i are much larger than would be expected for E_1, $E_1+\Delta_1$, given our expectation $\beta_i\leqslant 100$ K and given that the previously measured values of $\langle dE_i/dT\rangle_{\text{Low }T}$, measured over the lower-temperature interval, 77 K$\leqslant T\leqslant$300 K, all are in the range -0.6 meV/K $\leqslant dE_i/dT\leqslant -0.3$ meV/K, with average values approximately equal to -0.4 meV/K.[32–35] Our values can be made consistent with the previously measured values of $\langle dE_i/dT\rangle_{\text{Low }T}$ only by assuming very large values of β_i for the E_1 and $E_1+\Delta_1$ critical points. The required values are $\beta_{E_1}\approx 1000$ K and $\beta_{E_1+\Delta_1}\approx 350$ K. The second surprise, consistent with the requirement $\beta_{E_1}\approx 1000$ K, is that δ_{E_1} is approximately a factor of 2 larger than would be expected from the precision in our determination of $E_1(T)$. The large values of β_i required to make our values of dE_1/dT and $d(E_1+\Delta_1)/dT$ consistent with the previously measured low-temperature average values is even more striking, given that β_{E_0} must be less than 50 K to make our values for $E_0(T)$ consistent with the previously measured value $E_0(1.6K)=1.59$ eV,[36] which is well determined because $\Gamma_0(1.6K)<1$ meV. Also, $\beta_{E_2(\Sigma)}$ must be only about 100 K to make our value for $dE_2(\Sigma)/dT$ consistent with the average value -0.41 meV/K previously measured[32] over the temperature range 77 K$\leqslant T\leqslant$296 K.

TABLE V. Values of $E_i^{(0)}$ and η_i found by fitting our data to Eq. (10), along with δ_i in those fits.

CP	$E_i^{(0)}$ (eV)	η_i (meV/K)	δ_i (meV)
E_0	1.599	0.366	1.5
$E_0+\Delta_0$	2.502	0.340	9.7
E_1	3.615	0.824	7.1
$E_1+\Delta_1$	4.149	0.637	7.9
$E_2(X)$	5.252	0.919	11.0
$E_2(\Sigma)$	5.473	0.446	19.4

In light of the surprises discussed above, we refit $E_1(T)$ using Eq. (9), letting β_{E_1} be free. The value found for β_{E_1} is in excellent agreement with the value $\beta_{E_1}\approx 1000$ K found by requiring consistency between our data and the previously measured value for $\langle dE_1/dT\rangle_{\text{Low }T}$. Furthermore, this fit reduced δ_{E_1} by more than a factor of 2. In order to obtain formulas for the other $E_i(T)$ at least approximately valid below room temperature, we also refit them using Eq. (9), but keeping the β_i fixed at the values listed in Table VI, which provide good simultaneous fits to our data and to the previously measured values of $\langle dE_i/dT\rangle_{\text{Low }T}$. $\beta_{E_0+\Delta_0}$ was fixed to make $\langle d(E_0+\Delta_0)/dT\rangle_{\text{Low }T}$ same as $\langle dE_0/dT\rangle_{\text{Low }T}$. $\beta_{E_2(X)}$ was freed, since previously measured values for $\langle dE_2(X)/dT\rangle_{\text{Low }T}$ are not available. The resultant values for β_i, $E_i(0)$, and α_i are given in Table VI, along with the calculated and previously measured values of $\langle dE_i/dT\rangle_{\text{Low }T}$.

The temperature dependence of the linewidths $\Gamma_i(T)$ can be described as the sum of temperature-dependent and temperature-independent terms that add approximately quadratically,

$$\Gamma_i(T)=\sqrt{(\Gamma_i^{(0)}(T))^2+(\Gamma_i^{(1)})^2}. \tag{11}$$

The temperature-independent term contains contributions from alloy scattering, scattering off sample imperfections, experimental line broadening, and fictitious systematic broadening caused by the numerical differentiation of spectroscopic data. However, our sample was not an alloy and was of high quality, our experimental line broadening was

TABLE VI. Values of β_i, $E_i(0)$, and α_i obtained from fitting our data to Eq. (9), where all of β_i except β_{E_1} and $\beta_{E_2(X)}$ were fixed in such a way as explained in the text.

CP	Parameters in Eq. (9)				$-\langle dE_i/dT\rangle_{\text{Low } T}$ (meV/K)	
	β_i (K)	$E_i(0)$ (eV)	α_i (meV/K)	δ_i (meV)	From Eq. (9)	Others
E_0	180	1.565	0.406	1.8	0.30	0.3 [a]
$E_0+\Delta_0$	100	2.478	0.351	9.9	0.30	
E_1	924	3.467	1.468	2.9	0.45	0.55 [b], 0.5 [c], 0.23 [d]
$E_1+\Delta_1$	300	4.068	0.753	8.5	0.45	0.60 [e], 0.38 [c], 0.17 [d]
$E_2(X)$	382	5.124	1.154	10.1	0.62	
$E_2(\Sigma)$	80	5.447	0.456	19.6	0.41	0.41 [b]

[a]Reference 26.
[b]Reference 32.
[c]Reference 33.
[d]Reference 34.
[e]Reference 35.

less than 1 meV, and our technique of simultaneously numerically differentiating our data and our model formula for $\epsilon(\omega)$ eliminated the systematic broadening normally associated with numerical differentiation.[22,23] Therefore, we set $\Gamma_i^{(1)}$ equal to zero. We then approximated $\Gamma_i^{(0)}(T)$ by the usual expression[37,38] to obtain

$$\Gamma_i(T)=\Gamma_i(0)\left(1+\frac{2}{e^{\Theta_i/T}-1}\right), \tag{12}$$

where the factor multiplying $\Gamma_i(0)$ accounts for the effect of electron-phonon scattering with phonon frequency $k_B\Theta_i/\hbar$. However, because our data was restricted to temperatures $T\geqslant 296$ K and because the precision of our determination of the $\Gamma_i(T)$ was only of order $\pm 10\%$ or worse, we were unable to simultaneously determine physically reliable values of $\Gamma_i(0)$ and Θ_i from our data for each critical point. Also, there are no low-temperature measurements of the $\Gamma_i(T)$ to aid in determining those values. However, if one assumes Θ_i to have the same value Θ_{Av} for every critical point, which is true within the spirit of the model on which Eq. (12) is based, then one can hope to find Θ_{Av} to a good approximation by simultaneously fitting all of the $\Gamma_i(T)$. Upon doing that, one finds $\Theta_{Av}=480$ K within approximately $\pm 10\%$. The resultant fits are shown in Fig. 8; the resultant values for $\Gamma_i(0)$ are given in Table VII. The value of Θ_{Av} is surprisingly high, but should be approximately correct for Γ_{E_1}, $\Gamma_{E_1+\Delta_1}$, $\Gamma_{E_2(X)}$; separate best fits for those critical points give $\Theta_{E_1}=464$ K, $\Theta_{E_1+\Delta_1}=560$ K, and $\Theta_{E_2(X)}=419$ K. However, the value for $\Gamma_{E_0}(T)$ given by $\Theta=480$ K is 3.41 meV, which is much too large, suggesting that Θ_{E_0}, and probably $\Theta_{E_0+\Delta_0}$, should be considerable smaller. Aside from these problems, Eq. (12) yields calculated values for the $\Gamma_i(T)$ that are physically acceptable for all temperatures in that they are positive and increase monotonically with temperature.

V. OPTICAL PROPERTIES AS A FUNCTION OF PHOTON ENERGY AND TEMPERATURE

Having determined the $E_i(T)$ and $\Gamma_i(T)$ for the CPs between 1.4 eV and 6 eV, we proceeded to calculate $\epsilon(\omega,T)$. There are two ways to determine $\epsilon(\omega,T)$. The first, and more accurate method is to simply fit all of the data simultaneously and determine the parameters in terms of which $\epsilon(\omega,T)$ is expressed. The second method is to obtain $W(E)$ at room temperature and then calculate $\epsilon(\omega,T)$, taking into account the line broadening and energy shifts caused by changes in temperature. As was demonstrated previously,[10] the second method is useful in predicting the dielectric function at any temperature if temperature-dependence data are not available. Both methods are presented, and the results compared.

Following the first scheme, one can leave any number of

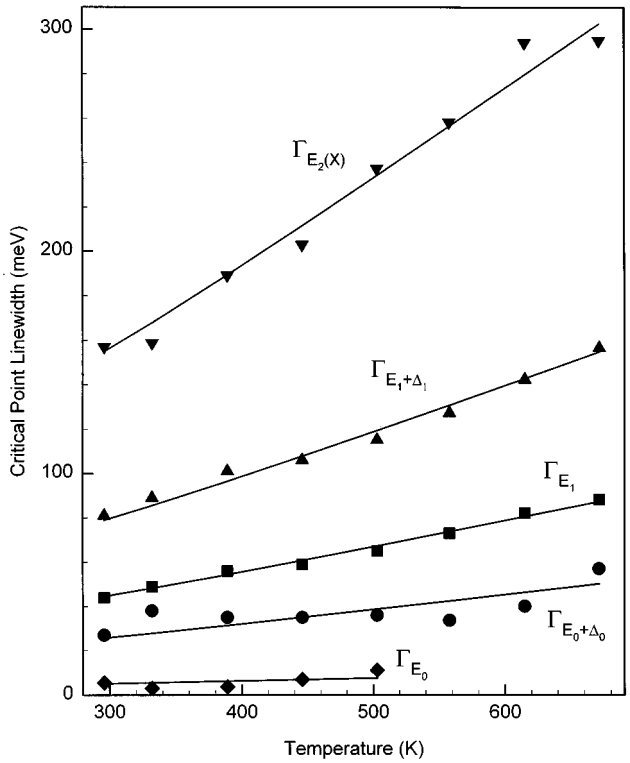

FIG. 8. CP linewidths as a function of temperature. The symbols show the values determined from fitting the data. The solid lines represent the fit by Eq. (12) with Θ_i constrained to have the same value at every CP.

TABLE VII. Values of $\Gamma_i(0)$ found from fitting our data to Eq. (12) with $\Theta_i = 480$ K for all critical points.

CP	$\Gamma_i(0)$ (meV)
E_0	3.41
$E_0+\Delta_0$	17.21
E_1	29.87
$E_1+\Delta_1$	52.91
$E_2(X)$	103.81

the $p_{\nu,n}$, $q_{\nu,n}$, and $r_{\nu,n}$ free at any given temperature with the remainder set to zero. Adding more parameters does not always improve the fit. We chose the free parameters in such a way as to obtain the best fit for a given total number of free parameters and to preserve the analytical nature of the joint density of the states at the CP's. When the room-temperature data were fitted with 15, 16, and 17 free parameters among the $p_{\nu,n}$, $q_{\nu,n}$, and $r_{\nu,n}$, σ_0 was 1.19%, 1.19%, and 1.15%, respectively. 15 free parameters were chosen among the $p_{\nu,n}$, $q_{\nu,n}$, and $r_{\nu,n}$, as is shown in Table VIII. The chosen parameters were relabeled as c_k, where $k=1,\ldots,15$. The c_k was expressed as a polynomial in T according to the equation

$$c_k = \sum_{m=0}^{m=N_k} c_{km} T^m, \tag{13}$$

where the c_{km} are temperature-independent parameters. This made it possible to fit simultaneously eight sets of data from room temperature to 671 K. N_k sets the maximum order polynomial for each c_k. Notice that $\epsilon(\omega,T)$ is linear in the c_{km}, which allows their values to be determined in a single iteration. As in the case of choosing free parameters among the $p_{\nu,n}$, $q_{\nu,n}$, and $r_{\nu,n}$, one can choose any number of the c_{km} to be free. The fractional error decreased as the total number of parameters increased. With all of the N_k set to 1, 2, 3, and 4, σ_0 was 5.1%, 2.92%, 2.68%, and 2.47%, respectively. Table IX shows the values for the c_{km} obtained in the fit with $N_k=3$. Though the entire set of the data was fit, for clarity only the data and the fit at 503 K are shown in Fig. 9. The solid lines in Fig. 9 show the resultant fit. The open and solid circles show the data. Once the dielectric function is found other optical properties such as the complex refractive indices, the reflectance, and the absorption coefficients are easy to find.[20]

TABLE VIII. The parameters c_k selected from among the coefficients $p_{\nu,n}$, $q_{\nu,n}$, and $r_{\nu,n}$; the zero values indicate parameters not allowed to be free, but fixed at zero.

Polynomial function	Order (n) 0	1
$p_{I,n}$	c_1	c_2
$q_{I,n}$	c_3	c_4
$r_{I,n}$	c_5	0
$p_{II,n}$	c_6	c_7
$q_{II,n}$	c_8	0
$p_{III,n}$	c_9	c_{10}
$q_{III,n}$	c_{11}	0
$p_{IV,n}$	c_{12}	0
$p_{V,n}$	c_{13}	0
$q_{V,n}$	c_{14}	0
$r_{V,n}$	c_{15}	0

TABLE IX. Values for the c_{km}.

c_k	c_{k0}	c_{k1}	c_{k2} (10^{-3})
c_1	640.37	−1.1401	0.90943
c_2	−164.44	0.31374	−0.28206
c_3	−366.14	0.69921	−0.60237
c_4	57.019	−0.15277	0.15819
c_5	13.067	−0.054714	0.058035
c_6	81.809	−0.038554	1.3146
c_7	2.2793	0.012159	−0.34833
c_8	−127.65	0.27216	−0.57596
c_9	539.06	0.63980	−0.99010
c_{10}	−63.787	−0.014749	0.29889
c_{11}	−208.49	0.37986	0.063641
c_{12}	92.823	0.17937	−0.19516
c_{13}	171.00	−0.50990	0.59542
c_{14}	−158.24	0.65169	−0.78345
c_{15}	822.67	−2.4282	2.5279

Previously, we presented a method for calculating the dielectric function $\epsilon^W(\omega,T)$ at any temperature from the room-temperature data.[10] Such a prediction was made possible due to the fact that $W(E)$ in Eq. (1) was found after fitting the room-temperature data with our model. Having measured the

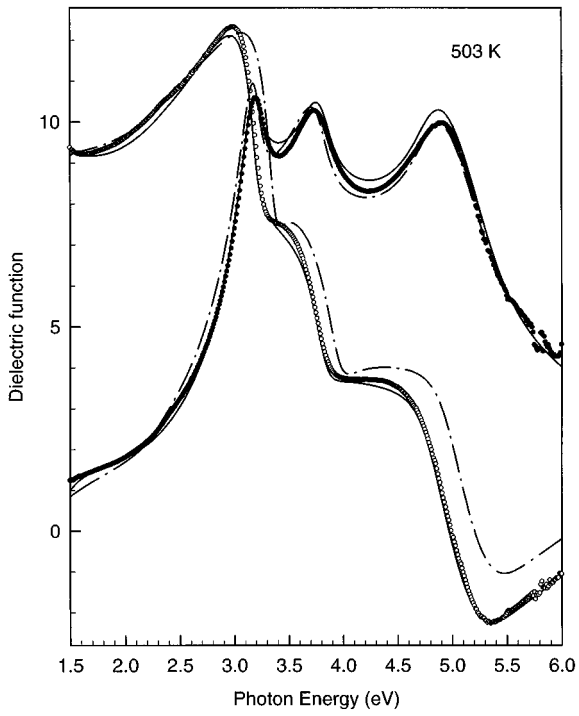

FIG. 9. Spectral data at 503 K. The open and solid circles are the real and imaginary parts of the dielectric function, respectively. The solid line shows the fit, and the dash-dotted line shows the result of a fit performed only at 296 K shifted in energy by the amount $E_1(503K)-E_1(296K)$ and altered to correspond to the linewidths at 503 K.

spectral data at elevated temperatures, we compared $\epsilon^W(\omega,T)$ with $L(\omega,T)$ at 503 K so that we might check the validity of this method. The general procedure to calculate $\epsilon^W(\omega,503)$ was the same as before. Briefly, $W(E)$ was obtained from fitting $L(\omega,296)$. The value for Γ_i at 503 K was calculated from the values in Table VII. The calculated result was shifted by -154 meV obtained from the difference between E_1 at 503 K and E_1 at 296 K. The dash-dotted lines in Fig. 9 show $\epsilon^W(\omega,503)$ calculated in this way. $\epsilon_2^W(\omega,503)$ is as close to $L_2(\omega,503)$ as is $\epsilon_2^F(\omega,503)$ obtained from the fit. $\epsilon_1^W(\omega,503)$ below the E_1 region is also as close to $L_1(\omega,503)$ as is $\epsilon_1^F(\omega,503)$. This indicates that the method is useful for predicting the refractive indices below E_1. $\epsilon_1^W(\omega,503)$ above E_1, however, is not as close to $L_1^W(\omega,503)$ as is $\epsilon_1^F(\omega,503)$.

VI. DISCUSSIONS AND CONCLUSIONS

One of the applications made possible by a knowledge of $\epsilon(\omega,T)$ is optical thermometry to determine the temperature of the sample surface during growth. There are two ways to do this. The first is to use $\epsilon(\omega,T)$ and the other is to use the CP energies and linewidths from the derivative spectra. Both methods have advantages and disadvantages. Yao *et al.* used the first method to determine the temperature of GaAs and found an uncertainty of ± 10 K.[14] More recently Heyd *et al.*[39] used the first method with a multilayer analysis to deduce the surface temperature of $GaAs/Al_xGa_{1-x}As$ heterostructures within ± 10 K using real time SE, even in the presence of an *a*-GaAs surface layer 3–4 nm thick. The advantage of this approach is that noise and a large frequency interval between data points are not a major obstacle in deducing the temperature. The weakness of this approach, however, is that either the sample surface must be in an ideal condition without the presence of an overlayer or a full multilayer analysis must be performed in real time; also, the variation of the dielectric function with sample quality must be minimal. Otherwise, the accuracy will drop. For example, consider the effect of an SiO_2 overlayer. The rms fractional error between $L(\omega_j,296)$ and $L(\omega_j,332)$ is 9.05%. That between $L(\omega_j,296)$ and $L(\omega_j,296)$ with 1.52 nm SiO_2 overlayer is also 9.05%. This indicates that the effect of a 1.52-nm oxide layer could mask the effect of a temperature change as large as 38 K if a multilayer analysis is not performed to subtract out the effect of the overlayer.

The second method is to determine the CP energies from fitting the derivative spectra and then deduce the temperature from results such as those shown in Fig. 7 and Table III. This method has the disadvantage of requiring data with a smaller frequency interval and with less noise, due to the enhancement of the noise in the derivative spectra. However, once this problem is overcome, this method provides accurate values for the temperature. The uncertainty in determining E_1 from fitting the derivative spectra is usually on the order of $\pm 2-4$ meV, depending on temperature. This corresponds to an uncertainty in temperrature of approximately ± 5 K at typical growth temperatures. Any small dependence of E_1 on the sample surface condition would add an extra 1 or 2 K uncertainty in the temperature. Similarly, one could use E_0 rather than E_1 to determine the temperature, or could use both E_0 and E_1 to determine temperature and alloy composition. The uncertainty in determining E_0 is no more than ± 2 meV, even at high temperatures, giving an uncertainty in T of no more than ± 6 K plus an uncertainty of about ± 1 K from uncertainty in surface quality. The CP linewidths could also be used to determine temperature, but with much less accuracy since $d\Gamma_{E_1}/dT$ is less than 0.2 meV/K and the uncertainty in determining Γ_{E_1} is much greater than that in determining E_1.

We have obtained the spectral data at elevated temperatures in the photon energy range between 1.3 eV and 6 eV. Our data obtained at room temperature differed by 10% from those of Arwin and Aspnes.[5] The large discrepancy is ascribed to differences in sample quality, surface condition and possibly instrumentation. Note that our sample was an MBE grown epilayer, whereas that studied by Arwin and Aspnes was a bulk sample. Despite the large differences in the dielectric functions obtained, our CP parameters were very close to theirs, especially for $E_0+\Delta_0$ and E_1. The spectral data at elevated temperatures showed the presence of an overlayer, but its effects were removed with the assumption of the linear decrease of the maximum value for $\epsilon_1(\omega)$ in the E_1 region. Our model, which was used to describe the spectral data of CdTe, was extended to describe the dielectric function as a function of temperature. With this model, the CP energies and linewidths were determined at selected temperatures, which were fitted to a function of temperature. The dielectric function was calculated as a function of temperature. Lastly, the previous method to predict the dielectric function at elevated temperatures was checked by comparing the prediction with the measured data at elevated temperature.

ACKNOWLEDGMENTS

The authors are grateful to D. E. Aspnes who provided the digitized data for CdTe. The authors are also grateful to the Advanced Research Projects Agency for its support under AFOSR Contract No. F49620-94-C-0080.

[1] S. S. Yoo, B. Rodricks, S. Sivananthan, J. P. Faurie, and P. A. Montano, Proc. SPIE **2228**, 201 (1994).

[2] Y. P. Chen, J. P. Faurie, and S. Sivananthan, Proc. SPIE **2228**, 54 (1994).

[3] D. E. Aspnes, IEEE J. Sel. Top. Quantum Electron. **1**, 1054 (1995).

[4] E. D. Palik, in *Handbook of Optical Constants of Solids*, edited by E. D. Palik (Academic, New York, 1985), p. 409, and references therein.

[5] H. Arwin and D. E. Aspnes, J. Vac. Sci. Technol. A **2**, 1316 (1984).

[6] L. Viña, C. Umbach, M. Cardona, and L. Vodopyanov, Phys. Rev. B **29**, 6752 (1984).

[7] S. Adachi, T. Kimura, and N. Suzuki, J. Appl. Phys. **74**, 3435

(1993).
[8] O. Castaing, R. Granger, J. T. Benhlal, and R. Triboulet, J. Phys.: Condens. Matter **8**, 5757 (1996).
[9] C. C. Kim, P. M. Raccah, and J. W. Garland, Rev. Sci. Instrum. **63**, 2958 (1992).
[10] C. C. Kim and S. Sivananthan, J. Appl. Phys. **78**, 4003 (1995).
[11] R. Sporken, Y. P. Chen, S. Sivananthan, M. D. Lange, and J. P. Faurie, J. Vac. Sci. Technol. B **10**, 1405 (1992).
[12] C. C. Kim, J. W. Garland, H. Abad, and P. M. Raccah, Phys. Rev. B **45**, 11 749 (1992).
[13] V. M. Bermudez and V. H. Ritz, Appl. Opt. **17**, 15 (1978).
[14] H. Yao, P. G. Snyder, and J. A. Woollam, J. Appl. Phys. **70**, 3261 (1991).
[15] H. Yao and P. G. Snyder, Thin Solid Films **206**, 283 (1991).
[16] D. E. Aspnes, in *The Accurate Determination of Optical Properties by Ellipsometry*, edited by E. D. Palik (Academic, New York, 1985), Chap. 5, p. 89.
[17] A. Ishizaka and Y. Shiraki, J. Electrochem. Soc. **1333**, 666 (1986).
[18] M. Wakagi, B. Hong, H. V. Nguyen, R. W. Collins, W. Drawl, and R. Messier, J. Vac. Sci. Technol. A **13**, 1917 (1995).
[19] G. N. Maracas, C. H. Kuo, S. Anand, and R. Droopad, J. Appl. Phys. **77**, 1701 (1995).
[20] C. C. Kim, J. W. Garland, and P. M. Raccah, Phys. Rev. B **47**, 1876 (1993).
[21] A. Savitsky and M. J. E. Golay, Anal. Chem. **36**, 1627 (1964).
[22] J. W. Garland, C. C. Kim, H. Abad, and P. M. Raccah, Phys. Rev. B **41**, 7602 (1990).
[23] J. W. Garland, C. C. Kim, H. Abad, and P. M. Raccah, Thin Solid Films **233**, 148 (1993).
[24] R. M. A. Azzam and N. M. Bashara, *Ellipsometry and Polarization Light* (North-Holland, New York, 1977).
[25] D. F. Edwards, in *Silicon (Si)*, edited by E. D. Palik (Academic, New York, 1985), p. 547.
[26] J. Camassel, D. Auvergne, H. Mathieu, R. Triboulet, and Y. Marfaing, Solid State Commun. **13**, 63 (1973).
[27] Y. P. Varshni, Physica (Utrecht) **34**, 149 (1967).
[28] P. Lautenschlager, M. Garriga, S. Logothetidis, and M. Cardona, Phys. Rev. B **35**, 9174 (1987).
[29] J. Jongler, C. Hetroit, P. L. Vuillermoz, J. Triboulet, J. Appl. Phys. **51**, 3171 (1980).
[30] A. Manoogian and J. C. Woolley, Can. J. Phys. **62**, 285 (1984).
[31] U. Piesbergen, Z. Naturforsch. **18A**, 141 (1963).
[32] M. Cardona and D. L. Greenaway, Phys. Rev. B **1**, 98 (1963).
[33] M. Cardona and G. Harbeke, J. Appl. Phys. **34**, 813 (1963).
[34] A. D. Brothers and J. B. Brungardt, Phys. Status Solidi B **99**, 291 (1980).
[35] M. Cardona, K. L. Shaklee, and F. M. Pollak, Phys. Rev. B **154**, 696 (1967).
[36] D. G. Thomas, J. Appl. Phys. **32**, 2298 (1961).
[37] L. Viña, S. Logothetidis, and M. Cardona, Phys. Rev. B **30**, 1979 (1984).
[38] P. Lautenschlager, P. B. Allen, and M. Cardona, Phys. Rev. B **33**, 5501 (1986).
[39] A. R. Heyd, R. W. Collins, K. Vedam, S. S. Bose, and D. L. Miller, Appl. Phys. Lett. **60**, 2776 (1992).